-Electronic Supplementary Information (ESI) -

Unveiling the influence of Fe_2O_3 nanoparticles on Cu_xO-TiO_2(B) nanofibers for dual Z-scheme electron transfer visible light photocatalysts: investigation on local atomic structures and electronic properties

Mani Preeyanghaa,[a] Chitiphon Chuaicham,[b] Sulakshana Shenoy,[b] Balakumar Vellaichamy,[b] Wei Li,[c] Kamaraj Manokaran,[d] Elumalai Varathan,[e] Bernaurdshaw Neppolian,[e] Bunsho Ohtani,[f] Keiko Sasaki,[b]* Karthikeyan Sekar,[b,e*]

[a]*Department of Physics and Nanotechnology, SRM Institute of Science and Technology, Kattankulathur, Chennai, 603203, India*

[b]*Department of Earth Resources Engineering, Faculty of Engineering, Kyushu University, 744 Motooka, Nishiku, Fukuoka 819-0395, Japan*

[c]*School of Engineering, Institute for Materials & Processes, The University of Edinburgh, Robert Stevenson Road, Edinburgh EH9 3FB, United Kingdom.*

[d]*Department of Chemistry, University of Manitoba, Winnipeg, Manitoba R3T 2N2, Canada*

[e]*Department of Chemistry, SRM Institute of Science and Technology, Kattankulathur, Chennai, 603203, India*

[f]*Institute for Catalysis, Hokkaido University, Sapporo 001-0021, Japan*

*Corresponding Author: Email: keikos@mine.kyushu-u.ac.jp; kart@mine.kyushu-u.ac.jp.

2.3. Characterization

The crystal information for the synthesized products was measured using a Rigaku Ultima IV powder X-ray diffractometer (XRD) utilizing a Cu Kα radiation source. The elemental and chemical composition states of the products were analyzed using a ULVAC-PHI ESCA 5800 X-ray photoelectron spectrometer (XPS) with an Al Kα excitation source. The Cu_2O concentrations in the bulk were estimated using a Rigaku ZSX Primus II X-ray fluorescence (XRF) spectrometer in wavelength dispersive mode. The morphology of the synthesized products was obtained by ZEISS Ultra-55 field emission scanning electron microscopy (FE-SEM) and JEOL JEM-2100HCKM high-resolution transmission electron microscopy (HR-TEM). Brunauer-Emmett-Teller (BET) and Barrett-Joyner-Halenda (BJH) were carried out on Belsorp-Mini, Microtrac. The bandgap energy of the synthesized products was estimated using a Shimadzu UV-2450 UV−Vis diffuse reflectance spectrophotometer (DRS) equipped with an ISR-2200 integrating sphere attachment. The steady state photoluminescence (PL) spectra and time-resolved PL (TR-PL) spectra of the samples were acquired using a F-4500FL spectrophotometer and an Edinburgh Photonics FLS980 spectrometer. The ESR was executed on a Bruker ESP 300E EPR spectrometry with an X-band frequency of 8.75-9.65 GHz.

2.4. X-ray absorption spectroscopy (XAS)

Cu K-edge XANES and EXAFS spectra for the reference samples (Cu foil, CuO and Cu_2O) synthesized catalysts were recorded using the BL15 beamline of the Kyushu Synchrotron Light Research Center, Japan. The photon energies of the X-ray beam were adjusted from 8.9 to 9.2 keV using a Si(111) double-crystal monochromator. The samples were diluted with a high purity hexagonal boron nitride powder and mounted onto a sample holder using Kapton tape. The spectra for the samples were measured at room temperature in

transmission mode. The storage ring was operated at a beam current of 287.1 mA and energy of 1.40 GeV. Linear combination (LC) fitting was performed to process the obtained data by utilizing the Athena programme suite (Demeter ver. 0.9.26) within the IFEFFIT software package.

2.5. Reversed double-beam photoacoustic spectroscopy (RDB-PAS)

A sample container containing ~200 mg of synthesized products was placed in a PAS cell equipped with an electret condenser microphone and quartz window on the upper side, which was infused with methanol-saturated N_2 gas for 30 min before being firmly closed. A grating monochromator attached to a Xe lamp was controlled at 80 Hz by a light chopper that transmitted a beam of light over the wavelength range of 650−350 nm via a cell window and the PA signal was monitored using a digital lock-in amplifier. Based on the amount of photoabsorption change for accumulated electrons, the energy-resolved distribution of electron traps (ERDT)/conduction-band bottom (CBB) patterns were measured for the synthesized samples.

2.6. Photoelectrochemical characterization

The electrochemical impedance spectroscopy (EIS), transient photocurrent (TPC) response and Mott–Schottky (M-S) plots of the synthesized products were measured using an Autolab potentiostat electrochemical workstation. A three-electrode cell system was used comprising a Pt wire counter electrode, Hg/Hg_2SO_4 reference electrode and glassy carbon (GC) working electrode in 0.5 M Na_2SO_4 electrolyte solution. The working electrode was prepared as follows: 5 mg synthesized product was uniformly dispersed in 0.5 mL Nafion containing 1:1 v/v of a water/ethanol mixture. After 30 min of ultrasonication, 5 μL of homogeneous colloidal solution was drop cast onto the GC electrode (3 mm diameter) and dried at ambient temperature. EIS Nyquist plots were recorded with a 10 mV AC signal in the frequency range

of 100 kHz to 0.1 Hz. The light source used for measuring the TPC response was a 200 W Hg-Xe arc lamp. M-S measurements were made by scanning the potential from − 1.0 to 1.0 V.

2.7. Trimethoprim (TMP) photocatalytic degradation experiments

The synthesized products (20 mg) were uniformly dispersed in 50 mL of 0.163 mM TMP solution in a quartz cell photoreactor using an ultrasonicator. The reaction mixtures were agitated in the dark for 60 min to establish adsorption-desorption equilibrium. After that, 500 W Xenon lamp (USHIO optical module) was used to irradiate the reaction mixtures. The samples were collected at regular intervals and filtered using a CPO20AN filter for high-performance liquid chromatography (HPLC) analysis. The TMP removal efficiency was computed using Eq. (1) as follows:

$$TMP\ removal\ (\%) = \frac{TMP(initial) - TMP(final)}{TMP(initial)} * 100 \qquad (1)$$

where the initial and final molar concentrations of TMP denote the concentrations at the beginning and end of the reaction, respectively.

Moreover, the radical trapping experiments were carried out under similar conditions as for the photocatalytic tests, with the exception that 0.1 mM scavengers were introduced before the reaction. The scavengers employed in these experiments were isopropyl alcohol (IPA), ethylenediaminetetraacetic acid (EDTA), and p-benzoquinone (BQ).

2.8. Chromatography conditions

The TMP concentration was scrutinized using a Jasco UV-2075Plus Intelligent UV–Vis Detector HPLC System with a Shodex Silica C18 M-4E HPLC Column (5 µm, 4.6 x 250 mm) measured at a wavelength of 254 nm. The mixture was separated at 25 °C with selectivity (α1-2.42, α2-1.47) and pressure (min 0.2 MPa, max 20 MPA). The eluent comprised 60:10:30 (v/v/v) acetonitrile–water–formic acid (25 mM) with a 0.6 mL·min^{-1} flow rate. Before

identification of the reaction products via the photocatalysis process, HPLC was calibrated for TMP using reference compounds (hydroquinone, benzoquinone, fumaric, maleic and oxalic acids).

Liquid chromatography–mass spectrometry (LC−MS/MS, Agilent 6545 LC/Q-TOF) with an Agilent ZORBAX RRHD Eclipse Plus (C18, 2.1 mm, 150 mm, 1.8 μm) analytical column was used to identify the TMP products. The gradient elution used a mobile phase A composed of 0.1% formic acid in water and methanol at 95:5 (v/v) and the mobile phase B was composed of acetonitrile. The injection volume was 10 μL, the flow rate was 0.4 $mL \cdot min^{-1}$, and the column temperature was 25 °C. The TMP products were analyzed in the positive ion mode (ESI+) with a mass scan range of 100–1000 m/z.

2.9. Photocatalytic hydrogen production

Typically, 20 mg of synthesized products was uniformly dispersed in 50 mL of distilled water containing 2 mL of methanol as a sacrificial electron donor using an ultrasonicator. Prior to UV-Vis light irradiation, the N_2 gas was continuously purged in a sealed quartz photoreactor for 60 min to remove all the dissolved oxygen from the reaction mixture. The evolved gas was collected in a 1 mL airtight syringe at a periodic interval and analyzed using gas chromatography.

Table S1. EXAFS Fitting parameters for CTNF-2 and CTNF-2(NS) nanocomposites.

Samples	Shell	Atom type	C.N.[a]	R (Å)[b]	ΔE^o (eV)[c]	σ^2 (10^{-3}, Å^2)[d]
CTNF-2	1st	Cu-O	4.084	1.97	0.129	0.009
	2nd	Cu-Ti	1.468	2.52	0.046	0.009
CTNF-2(NS)	1st	Cu-O	4.356	1.94	-0.907	0.006
	2nd	Cu-Ti	0.764	2.47	-0.907	0.006

[a] Coordination numbers. [b] Distance. [c] Threshold energy difference. [d] Debye-Waller factor.

Table S2. Elemental atomic % of the CTNF-2 and CFTNF-2 nanocomposites based on STEM-EDX and XPS analysis.

Elements	EDX-Atomic %		XPS-Atomic %	
	CTNF-2	CFTNF-2	CTNF-2	CFTNF-2
Ti	41.83	35.48	44.55	33.39
Cu	19.83	17.39	5.67	9.26
Fe	-	1.9	-	3.23
O	38.34	45.22	49.78	54.11

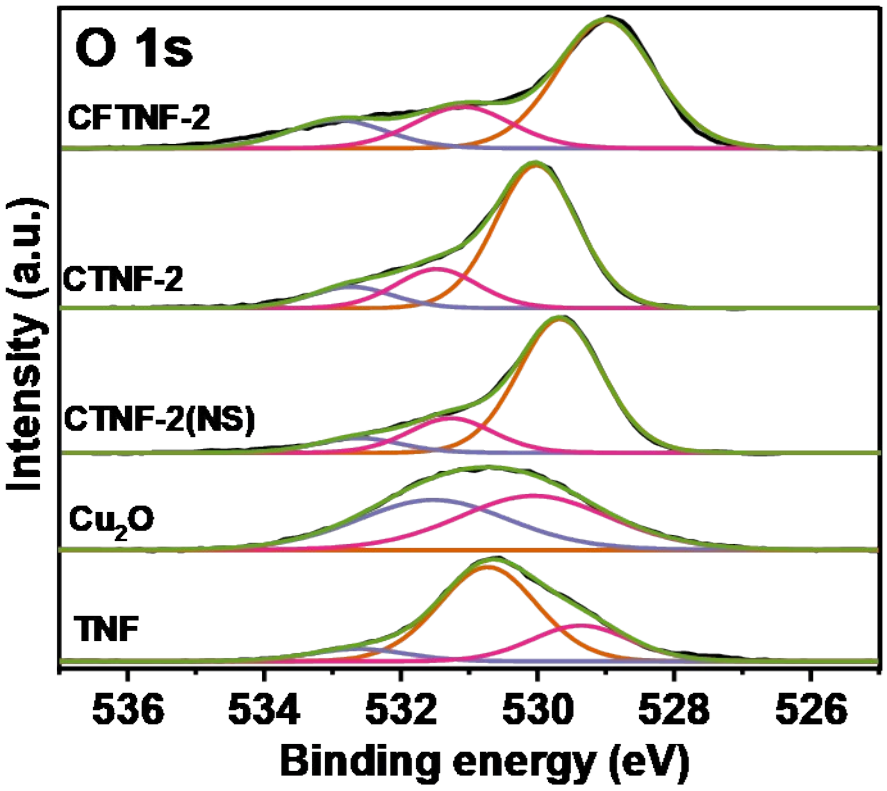

Fig. S1. Core level O 1s XPS spectra of the TNF, Cu_2O, CTNF-2, CTNF-2(NS) and CFTNF-2 nanocomposites.

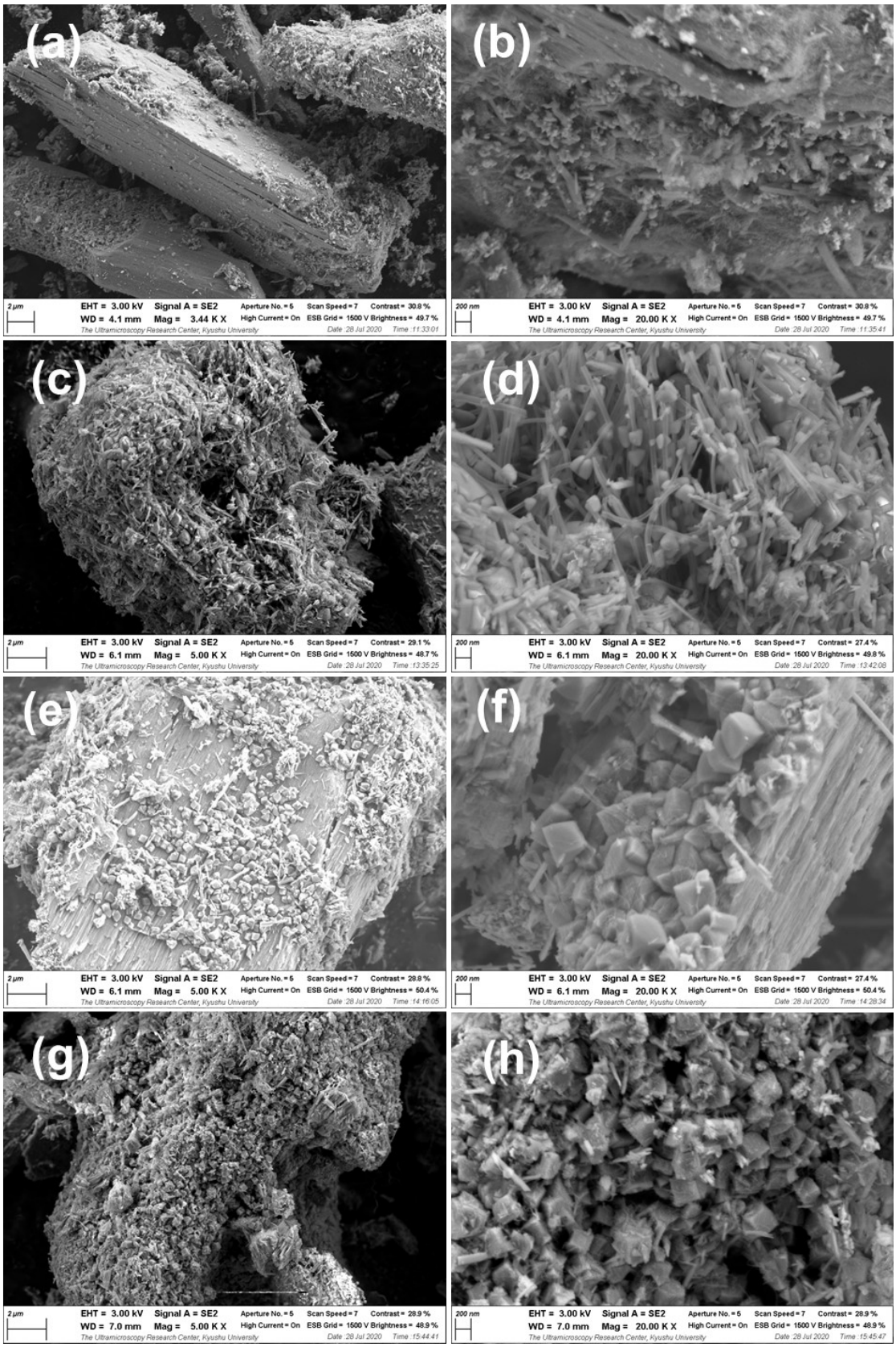

Fig. S2. FE-SEM images of (a, b) CTNF-1, (c, d) CTNF-3, (e, f) CTNF-5, (g, h) CTNF-10 nanocomposites.

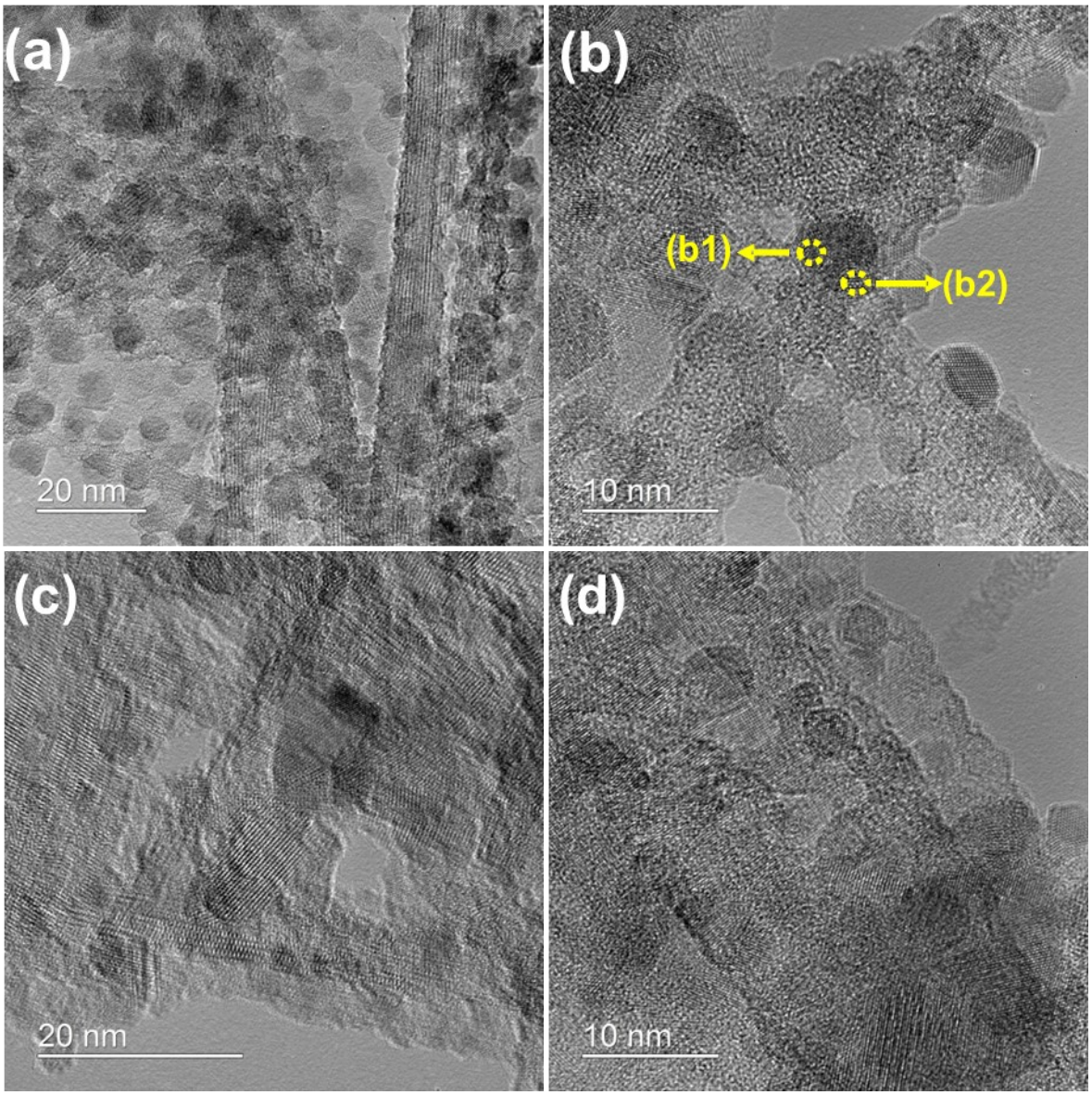

Fig. S3. HR-TEM images of CFTNF-2 nanocomposites

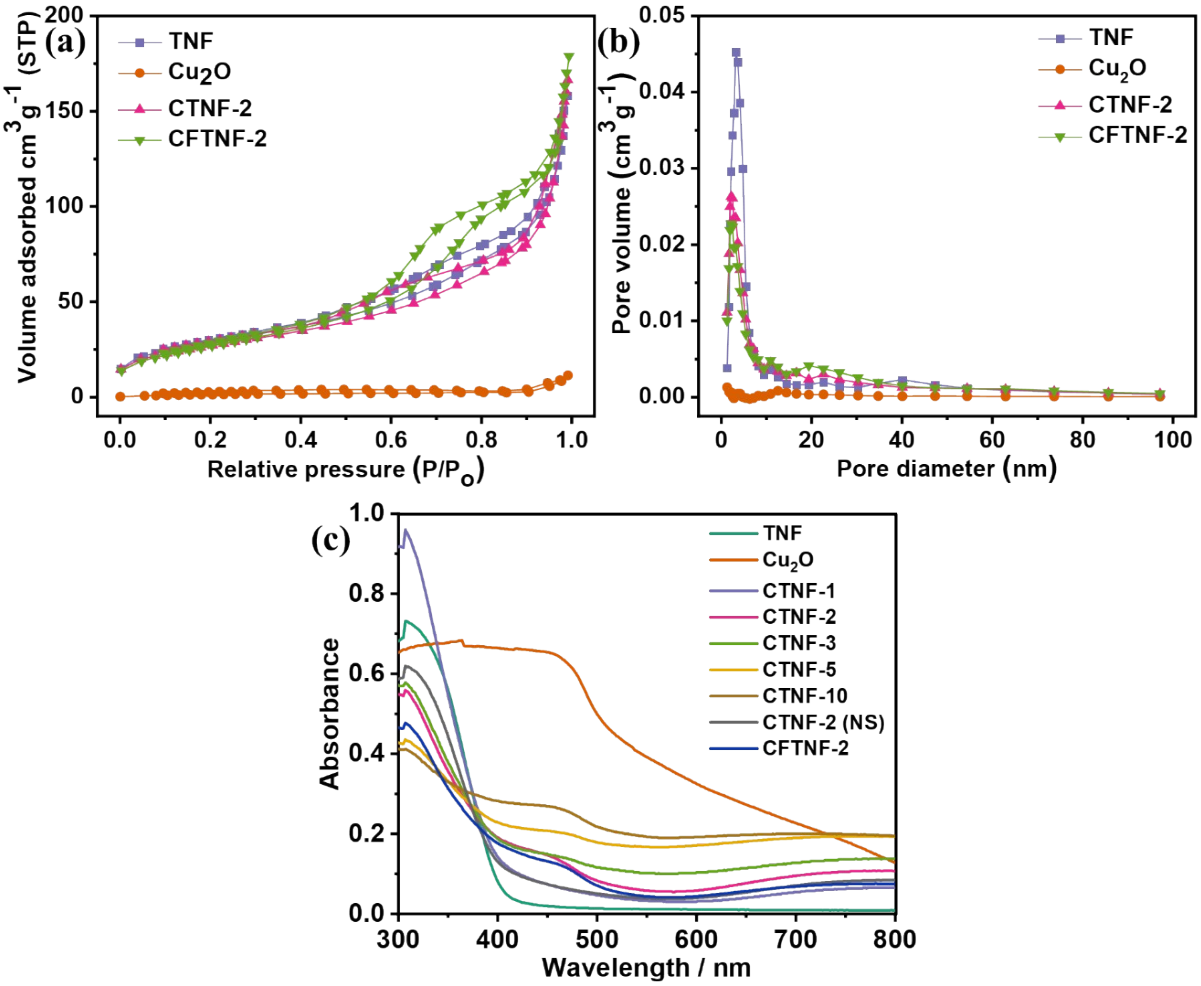

Fig. S4. (a) BET and (b) BJH plots of TNF, Cu_2O, CTNF-2 and CFTNF-2 nanocomposites. (c) UV–Vis DRS spectra of TNF, Cu_2O, CTNF-x, CTNF-2(NS) and CFTNF-2 nanocomposites.

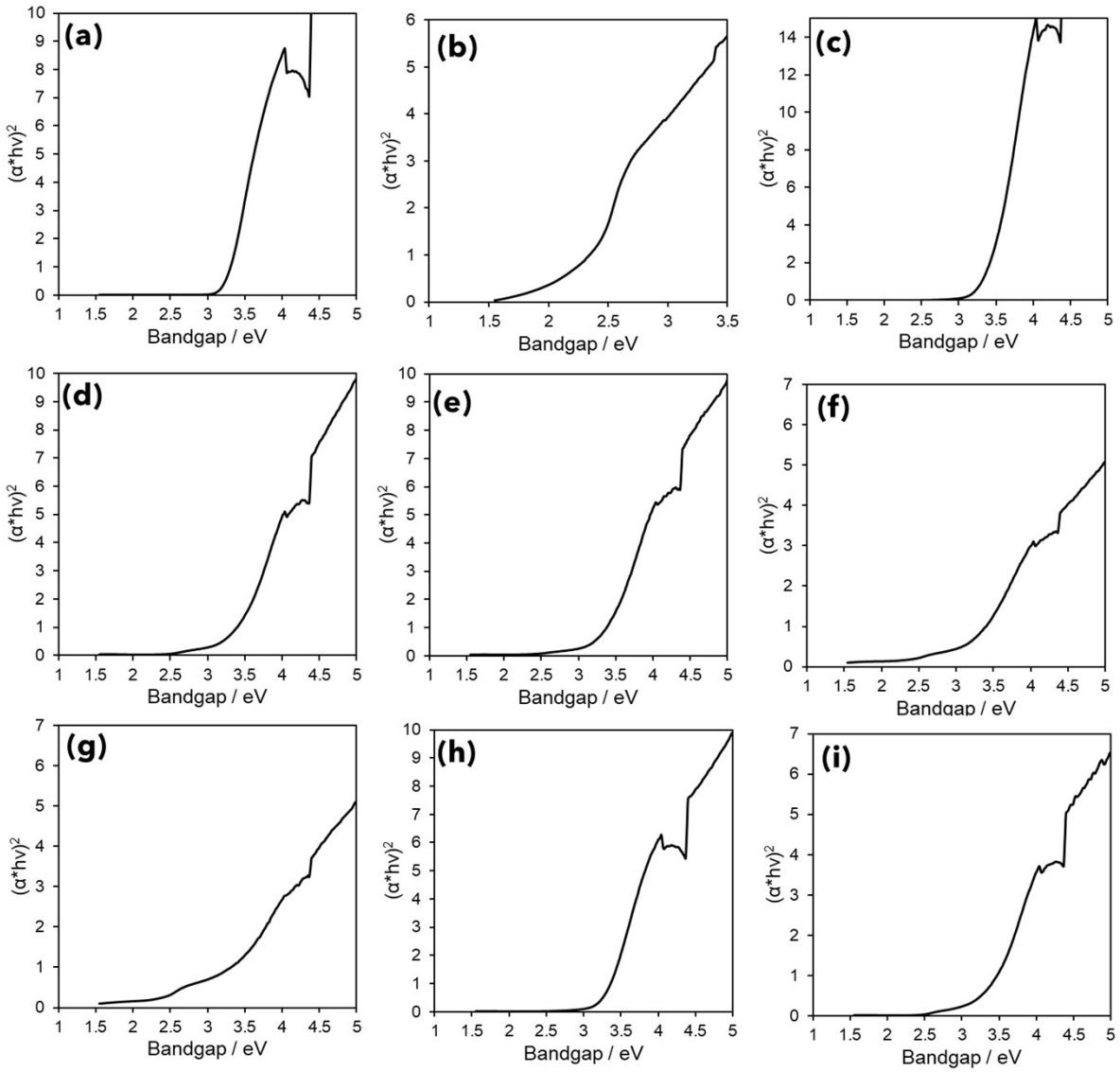

Fig. S5. Tauc plot of (a) TNF, (b) Cu_2O, (c) CTNF-1, (d) CTNF-2, (e) CTNF-3, (f) CTNF-5, (g) CTNF-10, (h) CTNF-2(NS) and (i) CFTNF-2 nanocomposite.

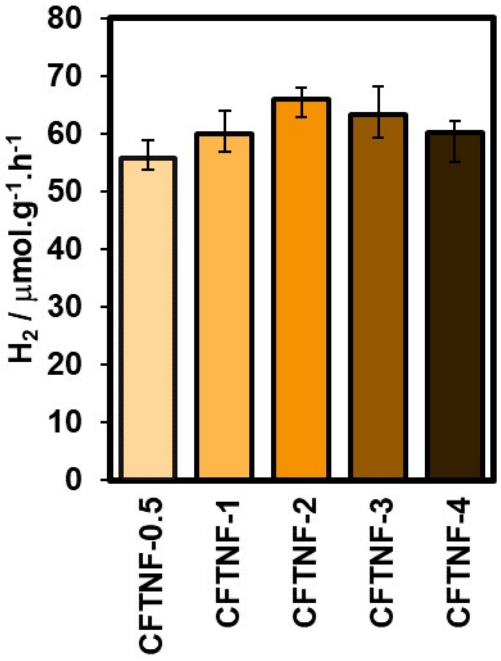

Fig. S6. Optimisation of Iron content in CTNF nanocomposites over photocatalytic H_2 production performance.

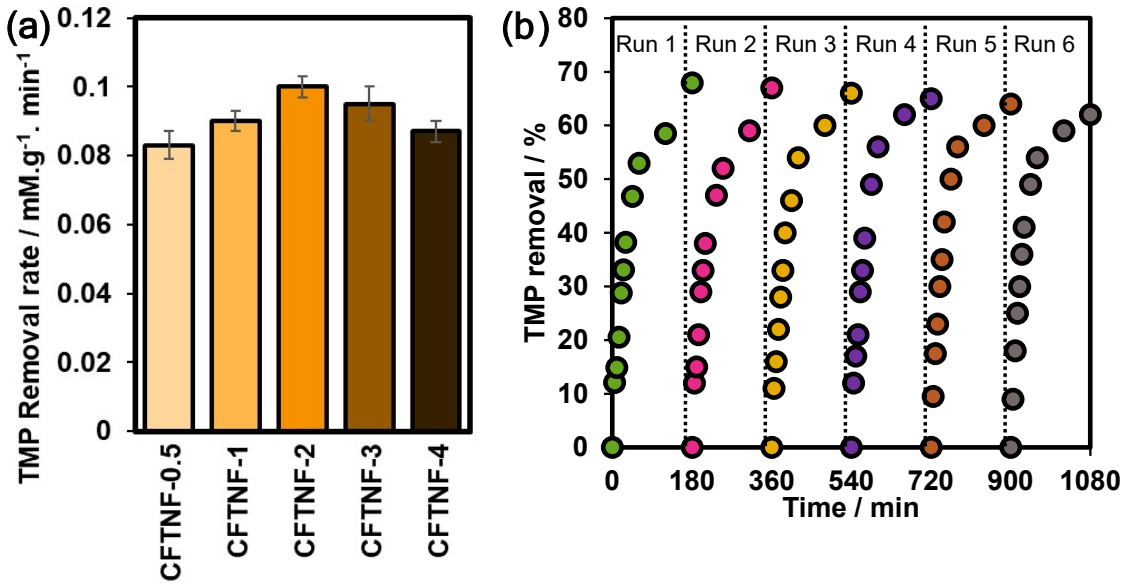

Fig. S7. Photocatalytic TMP degradation performance (a) Optimisation of Iron content in CTNF nanocomposites and (b) Reusability of CFTNF-2 nanocomposites.

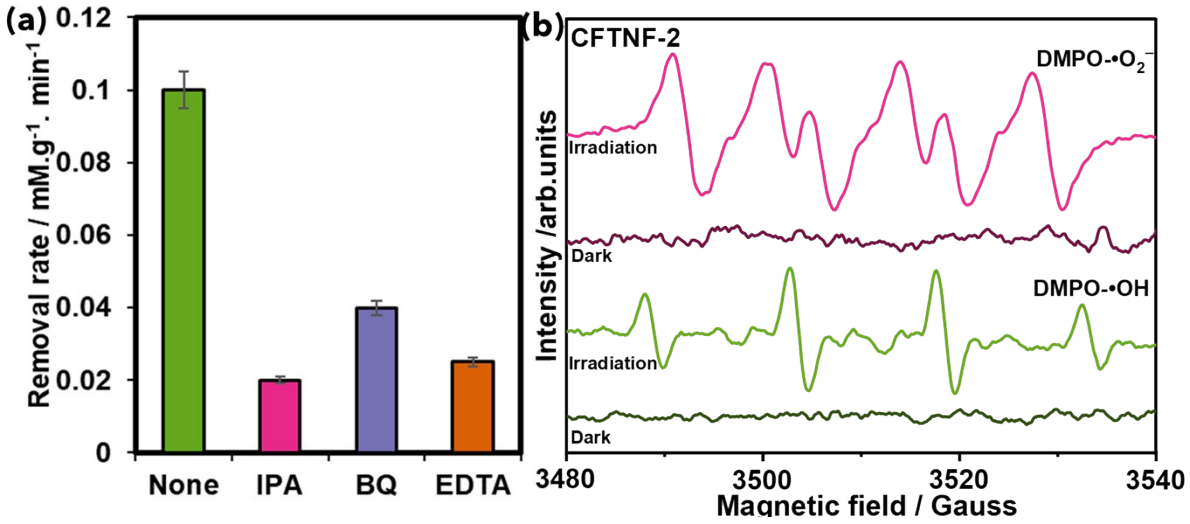

Fig. S8. (a) Reactive trapping experiment over CFTNF-2 nanocomposite and (b) ESR spectra of DMPO-•O_2^- and DMPO-•OH adducts under dark and light irradiation with CFTNF-2 nanocomposites.

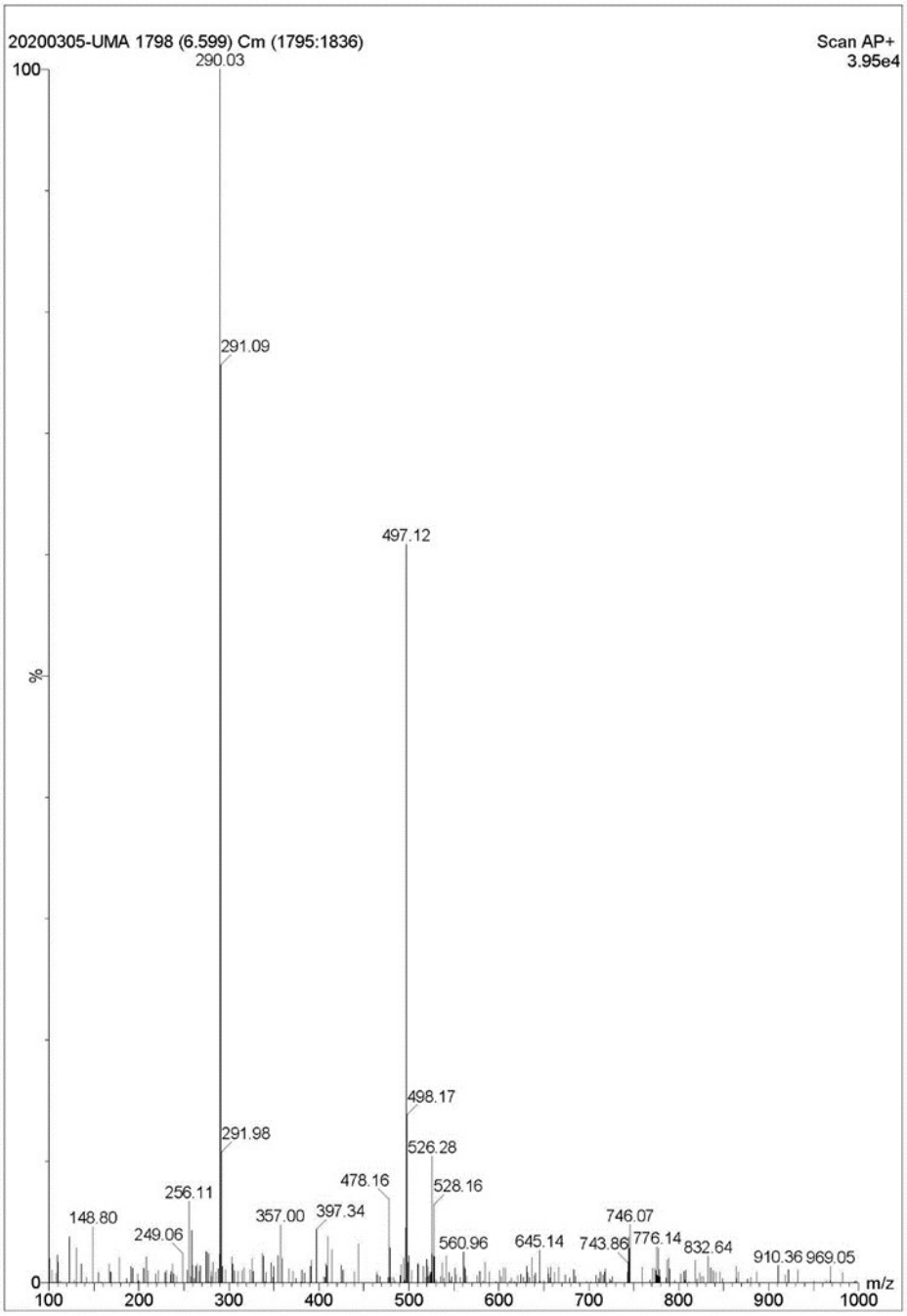

Fig. S9. LC−MS/MS spectra of TMP.

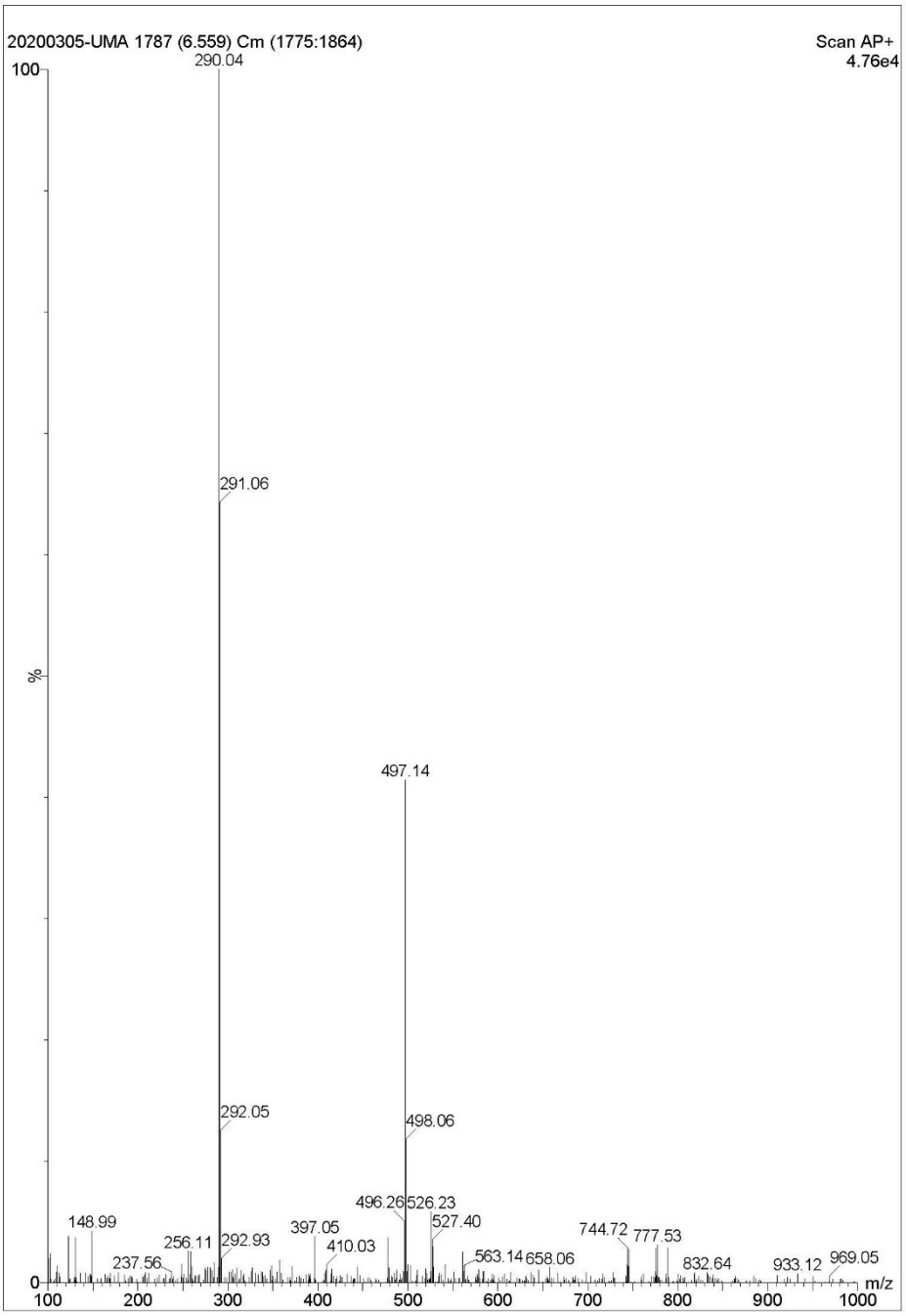

Fig. S10. LC−MS/MS spectra of TMP transformation products (5 min) over CFTNF-2 nanocomposite.

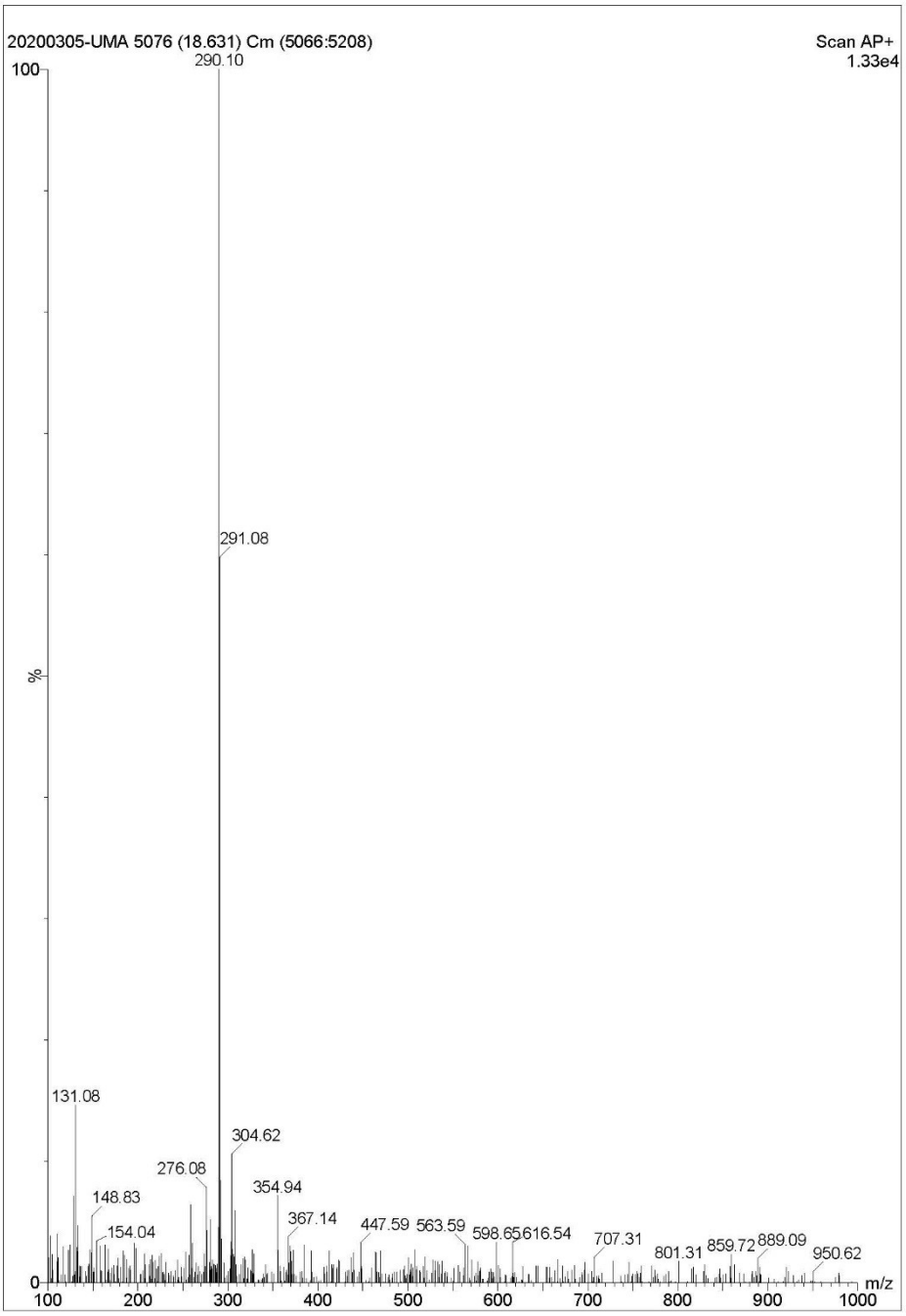

Fig. S11. LC−MS/MS spectra of TMP transformation products (30 min) over CFTNF-2 nanocomposite.

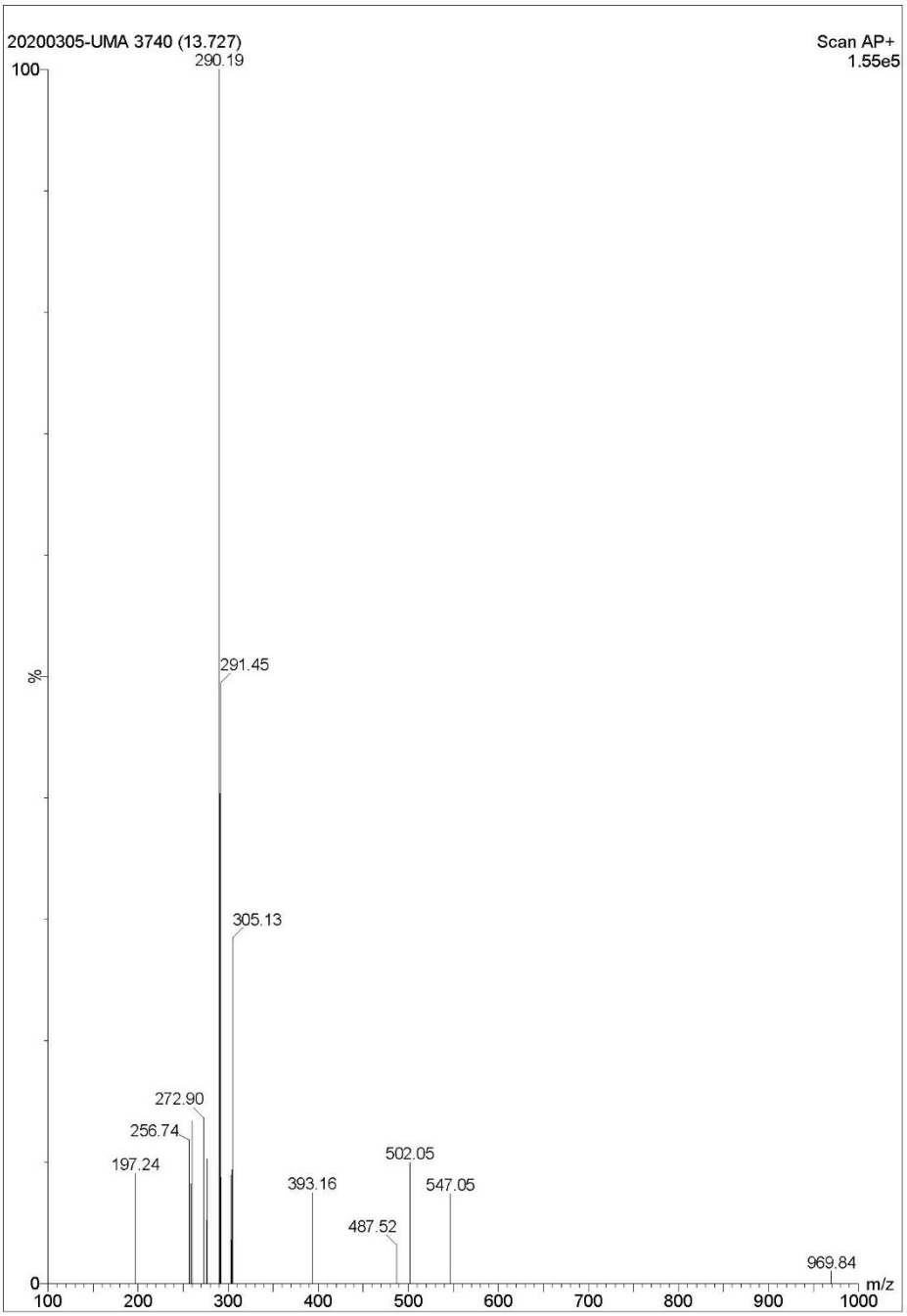

Fig. S12. LC−MS/MS spectra of TMP transformation products (60 min) over CFTNF-2 nanocomposite.

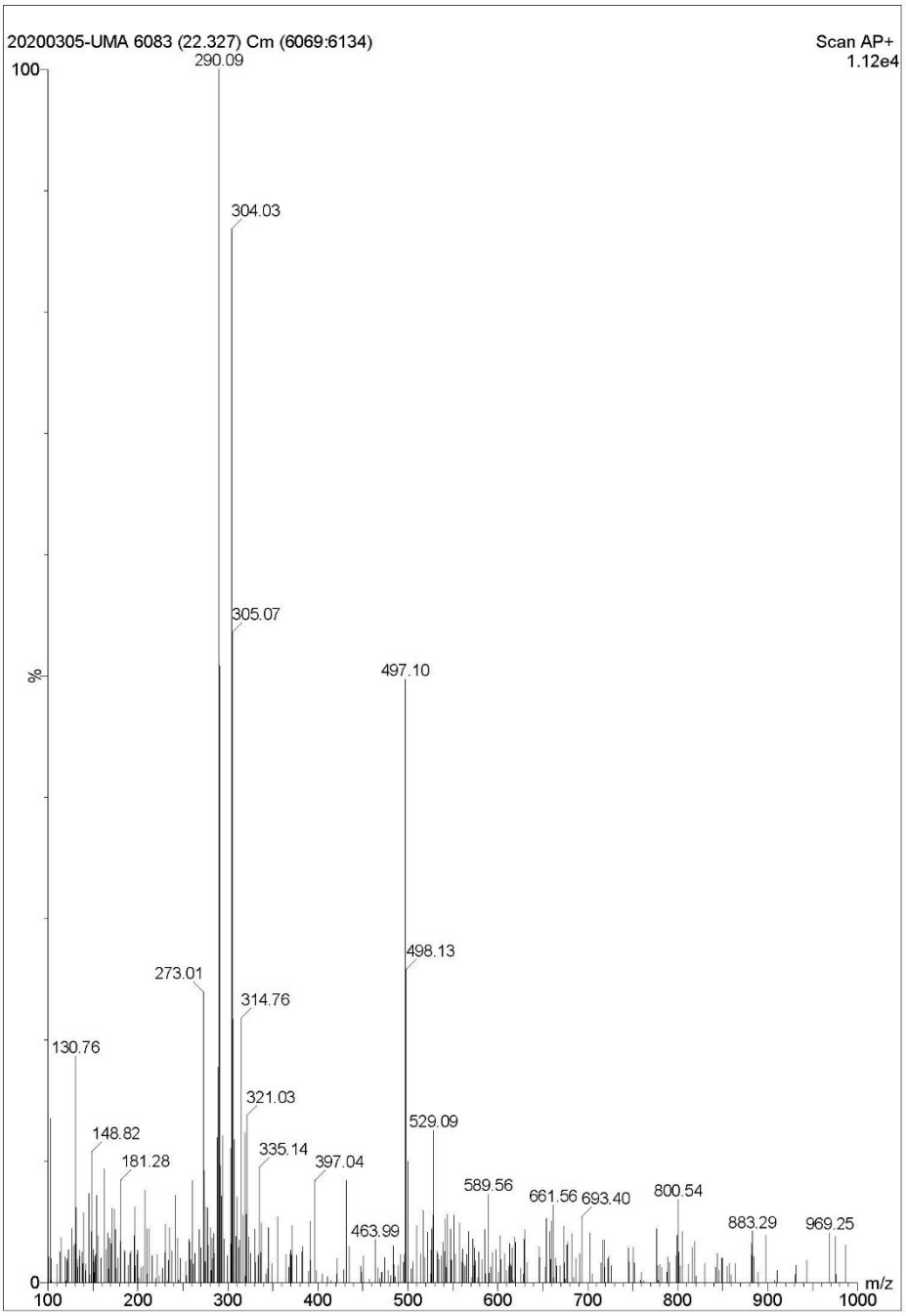

Fig. S13. LC−MS/MS spectra of TMP transformation products (180 min) over CFTNF-2 nanocomposite.

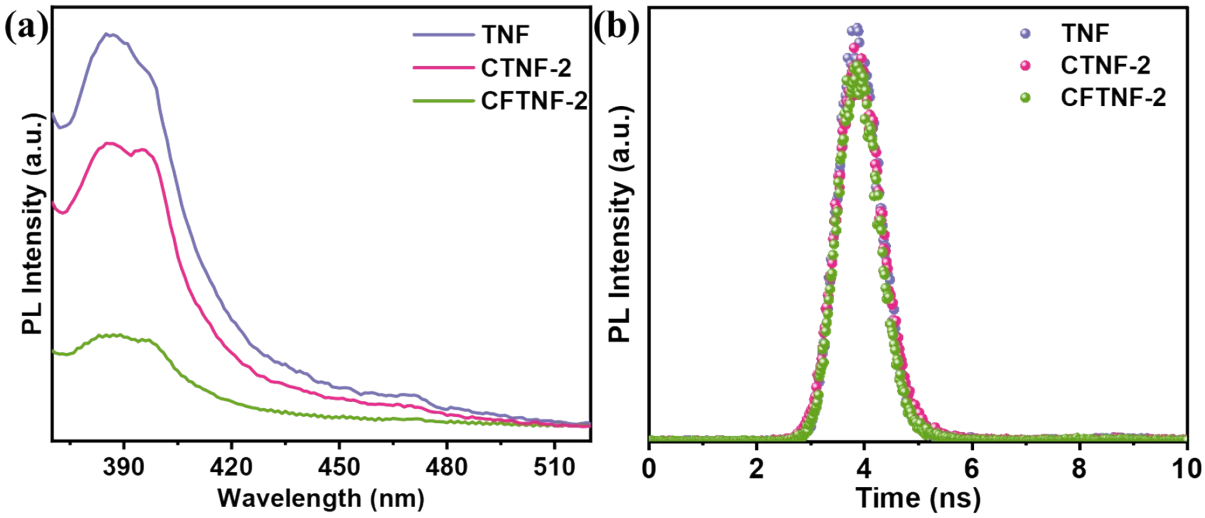

Fig. S14. (a) PL and (b) TR-PL spectra of TNF, CTNF-2 and CFTNF-2 nanocomposites.

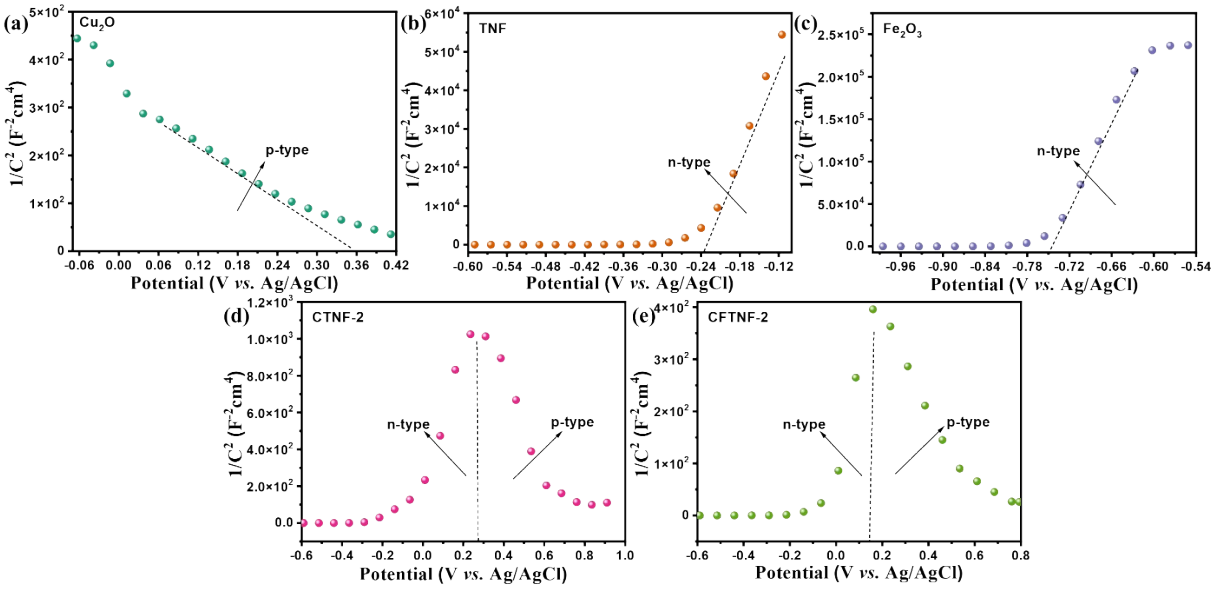

Fig. S15. Mott-Schottky plots of (a) Cu_2O, (b) TNF, (c) Fe_2O_3, (d) CTNF-2, and (e) CFTNF-2 nanocomposites.